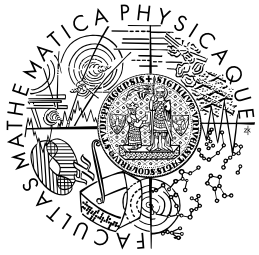

FACULTY
OF MATHEMATICS
AND PHYSICS
Charles University

BACHELOR THESIS

Valeriia Tynianskaia

Energy balance of corona in black-hole accretion disks

Astronomical Institute of Charles University

Supervisor of the bachelor thesis:	Mgr. Michal Bursa, Ph.D.
Study programme:	Physics
Study branch:	General physics

Prague 2018

I declare that I carried out this bachelor thesis independently, and only with the cited sources, literature and other professional sources.

I understand that my work relates to the rights and obligations under the Act No. 121/2000 Sb., the Copyright Act, as amended, in particular the fact that the Charles University has the right to conclude a license agreement on the use of this work as a school work pursuant to Section 60 subsection 1 of the Copyright Act.

In ..... date ..... signature of the author

I dedicate this thesis to my supervisor Michal Bursa and would like to thank him for all the guidance and patience. I also would like to thank consultant Michal Dovčiak for all of his priceless notes and help. I am very thankful for the opportunity to work with them.

Title: Energy balance of corona in black-hole accretion disks

Author: Valeriia Tynianskaia

Department: Astronomical Institute of Charles University

Supervisor: Mgr. Michal Bursa, Ph.D., Astronomical Institute of the Czech Academy of Sciences

Abstract: The presence of X-ray radiation that comes from the innermost regions of Active Galactic Nuclei indicates a presence of a hot gas component located close to the central black hole. The exact location and geometry of this so called corona is not known and various configurations are being considered in the literature. One of the suggestions for the geometry is a rather compact region located on the symmetry axis of the black hole (lamp-post model). Another variant is a layer that surrounds the accretion disk on both sides (slab model). Other models consider anything in between also in combination with a truncated disk.

One of the key questions connected with the corona that is not often addressed is how is the corona energized, i.e. where does it take energy from. Assuming the disk is the only source of energy in an accreting system and that its internal energy is partly radiated and partly used to support magnetic fields, we evaluate geometrical constraints on the corona from the energy conservation condition. Lastly, we try to investigate the total emitted spectrum of a system consisting of a central black hole, a thin accretion disk and a slab corona.

Keywords: active galactic nuclei, accretion disks, X-ray radiation of AGN

Contents

Introduction

For a long time in astrophysics nuclear fusion considered to be the main energy source. However, since the discovery of quasars (see e.g. Hazard et al., 1963, Schmidt, 1963), this point of view has changed. Quasars are known to be remarkably luminuos objects and for a large amount of time there was no exact explanation to their energy source. By now this problem was solved by the widely accepted concept of a supermassive black hole and a surrounding accretion disk.

It transpired, that a concept of accretion disk can be applied not only to quasars, but to number of astrophysical objects, such as young stellar objects, protostar, white dwarf, low-mass X-ray binary (LMXB), neutron star and a black hole. All of the named objects consider to be surronded by accretion disks.

We will restrict ourselves to active galactic nuclei (AGN). Active galactic nuclei generally include quasars, radio galaxies, Seyfert galaxies, starburst galaxies etc. The greatest interest of this particular thesis will be a black hole, which in many cases is in the center of a galaxy, and the surrounding accretion disk. Observed X-ray radiation from AGN can be explained by the existence of a hot matter located close to the central black hole named corona. The geometry of the corona is still unknown. However, there exist a number of hypotheses on possible geometries of the corona. In this thesis we will adopt slab geometry of the corona. We will assume an accretion disk to be the only source of energy in an accreting system consisting of the central black hole, an accretion disk and the corona. In further we will outline that geometry of the corona can be estimated from the energy conservation conditon in an accreting system.

In the first chapter we will give an overview of spectra from AGN, typical components of AGN X-ray spectra and the possible origin of these components. In the second chapter we will focus on energy balance between the black-hole accretion disk and the corona and examine slab geometry of the corona using energy conservation condition. Lastly, we will simulate a model spectrum for one of the possible geometries of the corona that will follow from energy balance equations.

Active galactic nuclei

1.1 Basic properties of AGN

A galaxy is a gravitationally bound system of stars, dust, gas and dark matter, that hosts a supermassive black hole in its center. Those galaxies which have the central region around the supermassive black hole rich on matter, can develop an actively accreting core, which is called active galactic nucleous (AGN). Galaxies with active nuclei are known to have extraordinary luminousity, which can vary on different timescales from several years to several hours. AGN also have wide radiation range and radiate from radio to X-ray and gamma-ray. Active galactic nuclei are considered to be a relatively small area in the very center of a galaxy. Due to an enormous amount of energy released by AGN, the central object of AGN is considered to be a black hole. Presence of such a compact and massive object as a black hole causes hightened activity of AGN especially in X-ray range. This activity becomes possible through an accretion process, which operates with gravitational energy and which can explain activities of many astronomical objects including quasars. Thus, accretion process becomes one of the most powerful sources of energy in astrophysics.

Nowadays, widely accepted model of AGN is a supermassive rotating black hole ($10^6_\odot$-$10^9_\odot$) surrounded by an accretion disk.

1.2 Accretion disks and accretion process

The accretion process operates with gravitational energy of gas which can be released when a particle of the gas infalls on a massive object. Further, the accretion disk plays the role of transforming gravitational energy into radiation. That is a brief rough model of accretion process and in what follows we will learn more about details.

One can imagine an accretion disk as a gaseous-like flat disk rotating around gravitating objects, such as protostars, neutron stars or black holes. Rotating substance in AGN disks is assumed to consist of partially ionized gas, mostly hydrogen. Accretion disk is considered to be geometrically-thin and optically-thick in z-direction. Those disks are called α-disks (Shakura and Sunyaev, 1973).

Since the gas in the disk undergoes differential rotation, viscous process will participate. Prove to be the case, viscosity plays at least two key roles in accretion process: angular momentum transfer and viscous heating of disk. As the gas in the disk rotates with the different velocities at different radii, there appears a friction (*viscosity*) between individual layers that provides gas heating. This gas heating via viscosity is called *viscous heating*. Heated gas then starts to radiate electromagnetic radiation and this radiation provides most of the luminousity of AGN.

Let us suppose that we put a test particle of the gas on a distance r in a point-mass potencial $\psi = -\frac{GM}{r}$ of the central object with the mass M. If the particle has angular momentum with respect to the central mass, it will start to rotate around the central object in an eccentric orbit. For specific angular momentum, $l = rv_\phi$, the specific energy of the test particle will be minimal when the orbit is

circular. Thus, gravitational force from central object is exactly balanced by the centrifugal force of the rotating gas as

$$\frac{GM}{r^2} = \frac{v_\phi^2}{r} = r\Omega^2 = \frac{l^2}{r^3}, \tag{1.1}$$

where G is gravitational constant, M the mass of the central object, r the distance from the center, Ω the angular speed of the gas particle, v_ϕ the linear speed of the gas particle.

Radius of the circular orbit is

$$r_{circ} = \frac{l^2}{GM}. \tag{1.2}$$

Thus, the gas rotates around the central object with the Keplerian angular velocity

$$\Omega = \Omega_K = \sqrt{\frac{GM}{r^3}}. \tag{1.3}$$

Linear velocity of the gas is

$$v_\phi(r) = r\Omega_K(r) \equiv \sqrt{\frac{GM}{r}}. \tag{1.4}$$

The test particle can never reach the center as long as its angular momentum is conserved. There is no mass accretion in this case, therefore, no energy can be radiated and cause luminousity of an accretion disk. In this way, one can see that viscosity is required as a mechanism to transfer angular momentum, which in further causes accretion disk to heat up and radiate.

We can imagine how viscosity works. Let us have two parallel shear flows, flow 1 (with greater velosity) and flow 2 (with smaller velosity). In such case momentum transfer will occure from flow 1 to flow 2 and, as a result, flow 2 will be accelerated and flow 1 will be decelerated. Thus, viscosity tends to produce uniform flows.

One can obtain a torque asserted on differentially rotating ring (see figure 1.1) as follows. Let us use cylindrical coordinates (r, ϕ, z) with the origin at the central star, where z-axis is considered to be perpendicular to the plane of the disk. As rotational velocity of annuli differs in the r-direction, the viscous force per unit area exerted in the φ-direction of the interface plane is (Kato et al., 1998)

$$t_{r\varphi} = \eta(\frac{\partial v_\varphi}{\partial r} - \frac{v_\varphi}{r}) = \eta r \frac{d\Omega}{dr}, \tag{1.5}$$

where r is the distance from annulus to the central object, $\eta = (\rho\nu)$ is a dynamical viscosity with ρ and ν the density and kinematic viscosity.

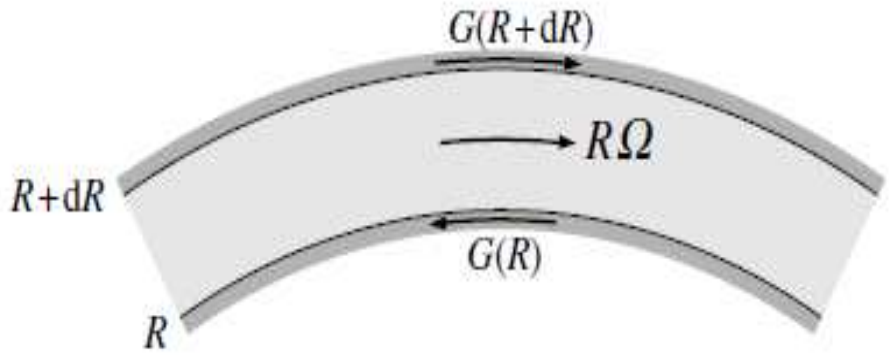

Figure 1.1: Differential viscous torque (Frank et al., 2002).

That is, the total torque exerted on the entire surface from outer annulus at $(r + \Delta r)$ is

$$G(r + \Delta r) = 2\pi(r + \Delta r) \int (r + \Delta r) t_{r\varphi} dz \approx 4\pi(r + \Delta r)^3 \eta H \frac{d\Omega}{d(r + \Delta r)}, \quad (1.6)$$

where H is a half-thickness of the annulus in z-direction (disk is geometrically thin when $H \ll r$).

If we redenote outer radius by r and inner radius by $r - \Delta r$, we obtain simplier form of equation (1.6)

$$G(r) = 2\pi r \int r t_{r\varphi} dz \approx 4\pi r^3 \eta H \frac{d\Omega}{dr}. \quad (1.7)$$

Now using equations (1.5) and (1.7) one can obtain basic equations for viscous disk evolution. Let us assume disk to be in energy balance and in hydrostatic equllibrium. We will use surface density given by

$$\Sigma = \int_{-\infty}^{\infty} \rho dz, \quad (1.8)$$

and vertically integrated viscous stress (see equation 1.5)

$$T_{r\varphi} \equiv \int_{-\infty}^{\infty} t_{r\varphi} dz = \nu \Sigma r \frac{d\Omega}{dr}. \quad (1.9)$$

We will consider the time evolution of an annulus of the disk at $r' \equiv r - \Delta r$ to r with $\Delta r \ll r$, where r' is inner radius and r is outer radius of an annulus.

Mass conservation of an annulus leads to an equation

$$\frac{\partial}{\partial t}(2\pi r \Delta r \Sigma) = (v_r \cdot 2\pi r \Sigma)_{r'} - (v_r \cdot 2\pi r \Sigma)_r \simeq -2\pi \Delta r \frac{\partial}{\partial r}(r \Sigma v_r), \quad (1.10)$$

where v_r is the radial velocity of the disk mass that considered to gradually drift inward by transferring its angular momentum outwards by viscosity (for accretion $v_r < 0$).

We can obtain the continuity equation using the limit of $\Delta r \to 0$

$$r\frac{\partial \Sigma}{\partial t} + \frac{\partial}{\partial r}(r\Sigma v_r) = 0. \tag{1.11}$$

Let us denote the mass flow rate by

$$\dot{M} \equiv -2\pi r v_r \Sigma. \tag{1.12}$$

Thus, we obtain

$$\frac{\partial \Sigma}{\partial t} = \frac{1}{2\pi r}\frac{\partial \dot{M}}{\partial r}. \tag{1.13}$$

The angular momentum transfer at the annulus is given by

$$\begin{aligned} \frac{\partial}{\partial t}(2\pi r \Delta r \Sigma r^2 \Omega) &= (v_r \cdot 2\pi r \Sigma \cdot r^2\Omega)_{r'} \\ &-(v_r \cdot 2\pi r \Sigma \cdot r^2\Omega)_r + \frac{\partial G}{\partial r}\Delta r \\ &\simeq -2\pi \Delta r \frac{\partial}{\partial r}(r\Sigma v_r r^2 \Omega) + \frac{\partial G}{\partial r}\Delta r, \end{aligned} \tag{1.14}$$

where $G(r)$ is from equation (1.7),

$$G(r,t) = 2\pi r^2 T_{r\varphi} = 2\pi r^3 \nu \Sigma \frac{d\Omega}{dr}, \tag{1.15}$$

with ν is the kinematic viscosity. In the limit $\Delta r \to 0$, we obtain

$$r\frac{\partial(\Sigma r^2\Omega)}{\partial t} + \frac{\partial}{\partial r}(r\Sigma v_r r^2 \Omega) = \frac{1}{2\pi}\frac{\partial G}{\partial r}. \tag{1.16}$$

With the help of the continuity equation (1.11), where we replaced v_r by $\dot{M}$, we have

$$\dot{M}\left[\frac{d}{dr}(r^2\Omega)\right] = -2\pi\frac{\partial}{\partial r}(r^2 T_{r\varphi}) = -2\pi\frac{\partial}{\partial r}\left(r^3\nu\Sigma\frac{d\Omega}{dr}\right), \tag{1.17}$$

where Ω is a function of r. Substituing equation (1.17) into equation (1.13), we obtain the following differential equations for Σ:

$$\frac{\partial \Sigma}{\partial t} = -\frac{1}{r}\frac{\partial}{\partial r}\left[\frac{\frac{\partial}{\partial r}(r^2 T_{r\varphi})}{\frac{d}{dr}(r^2\Omega)}\right] = -\frac{1}{r}\frac{\partial}{\partial r}\left[\frac{\frac{\partial}{\partial r}(r^3\nu\Sigma\frac{d\Omega}{dr})}{\frac{d}{dr}(r^2\Omega)}\right]. \tag{1.18}$$

In the case of point-mass potential, we find

$$\frac{\partial \Sigma}{\partial t} = -\frac{2}{r}\frac{\partial}{\partial r}\left[\left(\frac{r}{GM}\right)^{\frac{1}{2}}\frac{\partial}{\partial r}(r^2 T_{r\varphi})\right] \tag{1.19}$$

or

$$\frac{\partial \Sigma}{\partial t} = \frac{3}{r}\frac{\partial}{\partial r}\left[r^{\frac{1}{2}}\frac{\partial}{\partial r}\left(\nu\Sigma r^{\frac{1}{2}}\right)\right], \tag{1.20}$$

where we used equation (1.3) for Keplerian angular velosity Ω. All the above formulae were taken from Kato et al., 1998.

1.3 Disk energetics

In general, α disks could be fully described by the set of 11 equations. For us to derive energetic properties of an accretion disk and understand how it radiates, only two of them will be enough. In what follows, we will use angular-momentum conservation in an accretion disk and its energy balance. For Shakura-Sunyaev α disks we make the following assumptions:

1. The gravitational field in a disk is defined by a central object and the self-gravity of the disk is ignored.
2. The disk is steady.
3. The disk is axisymmetric.
4. The disk is geometrically thin ($H \ll r$) .
5. Rotational motion is dominant (Keplerian); $|v_r| \ll v_\varphi$.
6. Hydrostatic balance holds in the vertical direction.
7. The disk is optically thick in the vertical direction.

1.3.1 Angular-momentum conservation

Since, the disk is in a steady state, mass flow rate $\dot{M}$ is constant in space and time (see equation (1.12)) and we can integrate equation (1.17) (Kato et al., 1998),

$$\frac{\dot{M}}{2\pi} r^2 \Omega = -r^2 T_{r\varphi} + \text{const} = -r^3 \nu \Sigma \frac{d\Omega}{dr} + \text{const} \tag{1.21}$$

Adopting a boundary condition $T_{r\varphi}$ and setting $l = l_{\text{in}}$ =const at the inner edge of the disk, r_{in}, we have

$$\frac{\dot{M}}{2\pi}(l - l_{\text{in}}) = -r^2 T_{r\varphi} = -r^3 \nu \Sigma \frac{d\Omega}{dr}. \tag{1.22}$$

In a case of point-mass potential, $\psi = -\frac{GM}{r}$, $l = \sqrt{GMr}$ and $l_{\text{in}} = \sqrt{GMr_{\text{in}}}$ hold, thus

$$\begin{aligned} T_{r\varphi} &= -\frac{1}{2\pi}\sqrt{\frac{GM}{r^3}}\dot{M}\left(1 - \sqrt{\frac{r_{\text{in}}}{r}}\right) \\ \text{or} \quad \nu\Sigma &= \frac{\dot{M}}{3\pi}\left(1 - \sqrt{\frac{r_{\text{in}}}{r}}\right). \end{aligned} \tag{1.23}$$

1.3.2 Energy balance

Accretion disk converts potential energy of accreting gas to thermal energy via viscosity. That thermal energy will be then released as radiation. Let us define viscous heating rate per unit volume as $\rho\nu\left(r\frac{d\Omega}{dr}\right)^2$ (Lynden-Bell and Pringle, 1974), then the vertically intedrated heating rate per unit surface is

$$Q^+_{\rm vis} = \int_{-\infty}^{\infty} \rho\nu \left(r\frac{d\Omega}{dr}\right)^2 dz = \frac{9}{4}\nu\Sigma\Omega^2 = -\frac{3}{2}T_{r\varphi}\Omega, \tag{1.24}$$

where $\Omega = \Omega_K$ (see equation 1.3).

Accretion disk is cooling due to radiation from the disk surface. Since the disk is optically thick in the vertical direction (see Shakura-Sunyaev disks assumptions above),

$$\tau = \bar{\kappa}\rho H = \frac{\bar{\kappa}\Sigma}{2} \gg 1, \tag{1.25}$$

the disk gas emmits a blackbody spectrum with an effective temperature $T_{\rm eff}$, where τ is the optical depth and $\bar{\kappa}$ is the Rooseland opacity. The main opacity sources in high-temperature disks ($T \geq 10^4$K) are electron scattering and free-free absorbtion, therefore, Rooseland opacity is defined by

$$\bar{\kappa} = \kappa_{\rm es} + \kappa_{\rm ff} = \kappa_{\rm es} + \kappa_0\rho T^{-3.5}, \tag{1.26}$$

where $\kappa_{\rm es} = 0.4{\rm cm}^2{\rm g}^{-1}$, $\kappa_0 = 6.4\cdot 10^{22}{\rm cm}^2{\rm g}^{-1}$ for pure hydrogen plasmas.

Thus, we can define the cooling rate as the amount of emergent flux from a unit area of the surface,

$$Q^-_{\rm rad} = 2F = 2\sigma T^4_{\rm eff}, \tag{1.27}$$

where σ is the Stefan-Boltzmann constant, and the factor 2 represents radiaton from the two sides of the disk. In what follows, we will assume that the main energy transfer inside the disk is due to radiation. Let us define radiative flux in the z-direction as

$$F(z) = -\frac{4ac[T(z)]^3}{3\kappa(z)\rho(z)}\frac{\partial T}{\partial z}, \tag{1.28}$$

at each height, where a is the radiation constant ($\sigma = ac/4$). Thus, we can express the cooling rate of the temperature T_c at z=0,

$$Q^-_{\rm rad} = 2\frac{4acT_c^4}{3\tau} = \frac{32\sigma T_c^4}{3\tau}. \tag{1.29}$$

Therefore, the local energy balance at each radius is given by

$$Q^+_{\rm vis} = Q^-_{\rm rad}, \tag{1.30}$$

where heating is due to the viscosity (see equation(1.24)) and cooling is via the blackbody radiation.

Using equations (1.23), (1.24), (1.27) and (1.30), we obtain the emergent local flux as

$$F = \sigma T^4_{\rm eff} = \frac{3GM\dot{M}}{8\pi r^3}\left(1-\sqrt{\frac{r_{\rm in}}{r}}\right). \tag{1.31}$$

Thus, the effective temperature $T_{\rm eff}$ is

$$T_{\rm eff} = \left[\frac{3GM\dot{M}}{8\pi\sigma r^3}\left(1-\sqrt{\frac{r_{\rm in}}{r}}\right)\right]^{1/4}. \tag{1.32}$$

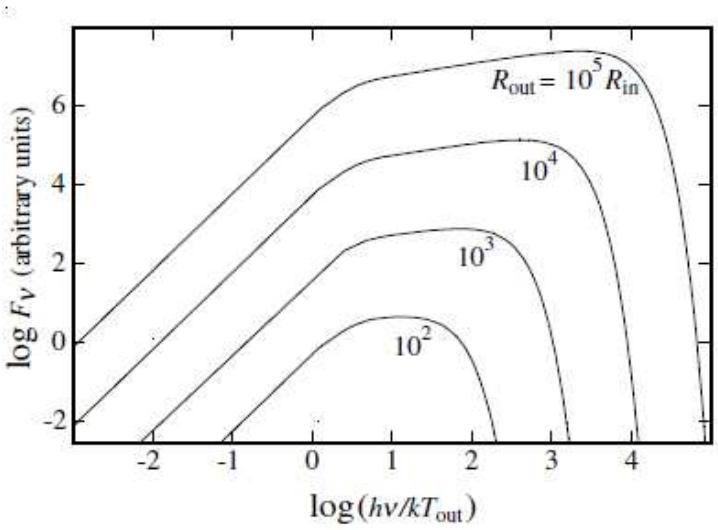

Figure 1.2: Accretion disk spectrum for different radii of the disks (Frank et al., 2002).

In an accretion disk the effective temperature of the disk has radial dependence. Thus, the inner area of the disk is hotter than the outer region. It becomes then straightforward that the total observable spectra of the disk are composed of multi-color blackbody spectra, where high-energy photons come from the inner region of the disk and low-energy photons come from the outer region.

Since, surface of the disk radiates locally as a multicolored blackbody:

$$B_\nu(r) = \frac{2h}{c^2} \frac{\nu^3}{e^{h\nu/k_B T(r)} - 1}, \tag{1.33}$$

one can calculate the observed flux F_ν of the disk by integrating the specific intensity $I_\nu = (B_\nu)$ of the disk over the surface of the disk (Kato et al., 1998)

$$F_\nu = \int I_\nu d\Omega = \frac{\cos i}{D^2} \int_{r_{\rm in}}^{r_{\rm out}} B_\nu 2\pi r dr, \tag{1.34}$$

where i is the inclination angle of the disk, Ω the solid angle subtended by the disk in the sky of the observer, D the distance to the disk.

Note that equation (1.32) defines the effective temperature distribution in equation (1.33). Since, the variation of temperature near to the inner edge has small influence on the overall structure of the spectra, we can define following approximation for the surface temperature of the disk

$$T = T_{\rm in} \left(\frac{r}{r_{\rm in}} \right)^{-p}, \tag{1.35}$$

where $T_{\rm in}$ is the temperature at $r = r_{\rm in}$, p the exponent adopted to be $\frac{3}{4}$ for the standard disk.

Thus, from equations (1.33), (1.35) the observed flux is

$$\begin{aligned} F_\nu &= \frac{\cos i}{D^2} 2\pi \left(-\frac{r_{\rm in}^2}{p} \right) T_{\rm in}^{2/p} \int B_\nu T^{-(2/p)-1} dT \\ &= \frac{\cos i}{D^2} \frac{4\pi h}{c^2} \frac{r_{\rm in}^2}{p} \left(\frac{k_B T_{\rm in}}{h\nu} \right)^{2/p} \nu^3 \int_{x_{\rm in}}^{x_{\rm out}} \frac{x^{(2/p)-1}}{e^x - 1} dx, \end{aligned} \tag{1.36}$$

where

$$x_{\rm in} = \frac{h\nu}{k_B T_{\rm in}} \quad \text{and} \quad x_{\rm out} = \frac{h\nu}{k_B T_{\rm in}} \left(\frac{r_{\rm out}}{r_{\rm in}}\right)^p. \tag{1.37}$$

In general, when one adopt the surface-temperature distribution to be $T \propto r^{-p}$, the observed flux of the disk becomes

$$F_\nu \propto \nu^{3-(2/p)} \quad \text{for} \quad \frac{k_B T_{\rm in}}{h} \left(\frac{r_{\rm in}}{r_{\rm out}}\right)^p \ll \nu \ll \frac{k_B T_{\rm in}}{h}, \tag{1.38}$$

(see equation (1.36)). Example of typical continuum spectra of the standard accretion disk is shown in figure 1.2.

1.4 AGN spectrum

1.4.1 Luminosity

Luminosity is the total amount of energy emitted per unit of time by an astronomicel object. One can derive a disk luminosity with the help of a test particle of unit mass rotating circularly at radius r. This particle has kinetic energy

$$K = \frac{1}{2} v_\varphi^2 = \frac{GM}{2r}. \tag{1.39}$$

The potencial energy is

$$U = -\frac{GM}{r} = -2K. \tag{1.40}$$

The excess energy that can be radiated of a particle with zero total energy falling from infinity to radius r is

$$0 - (U + K) = K = \frac{GM}{2r}. \tag{1.41}$$

Thus, the disk luminosity is given by

$$L_{\rm d} = \frac{GM\dot{M}}{2r_{\rm in}}. \tag{1.42}$$

Since we obtained equation for the emergent local flux in previous section (see equation (1.31)), we can also calculate disk luminosity from its flux as follows

$$L_{\rm d} = \int_{r_{\rm in}}^{\infty} 2F 2\pi r dr = \int_{r_{\rm in}}^{\infty} \frac{3GM\dot{M}}{2r^2} \left(1 - \sqrt{\frac{r_{\rm in}}{r}}\right) dr = \frac{GM\dot{M}}{2r_{\rm in}}, \tag{1.43}$$

In the case of accretion disks around the Schwarzschild black holes, $r_{\rm in} = \frac{6GM}{c^2}$, the disk luminosity becomes

$$L_{\rm d} = \frac{1}{12} \dot{M} c^2. \tag{1.44}$$

Generally we can write the radiation energy associated with the mass accretion rate as

$$L = \eta \dot{M} c^2, \tag{1.45}$$

where η is the efficiency, at which gravitational energy is converted to radiational energy.

Particles in the accretion disk rotating near a gravitating object of mass M and luminosity L are attracted inward by gravity of the central object and pushed outward by radiation pressure. Usually, when the luminosity of the central object is not large, the radiation-pressure force is smaller than the gravitational force and particles stay in the gravitational field of the object. As the luminosity increases for a fixed mass of the central object, the radiation-pressure force also becomes large and eventually overcomes the gravitational force, and gas particles are blown off. Thus, gas cannot accrete radially onto such an extremely luminous object. There exists a maximum possible luminosity, the *Eddington luminosity* $L_{\rm E}$.

Let us derive the Eddington luminosity for a spherical accretion flow of pure hydrogen. At distance r from a spherical accretion object of luminosity L, the radiaton flux (the amount of radiation energy flowing per unit time per unit area) is

$$f = \frac{L}{4\pi r^2}. \tag{1.46}$$

This energy flux carries a momentum flux of

$$\frac{1}{c} f = \frac{1}{c} \frac{L}{4\pi r^2}, \tag{1.47}$$

where c is the speed of light. Assuming the effective cross-section of an electron is the Thompson scattering cross-section $\sigma_{\rm T}$, the force imposed on each electron by radiation is

$$\frac{\sigma_{\rm T}}{c} f = \frac{\sigma_{\rm T}}{c} \frac{L}{4\pi r^2}. \tag{1.48}$$

Simultaneously, the gravitational force $F_{\rm g}$ asserted on each hydrogen atom is

$$F_{\rm g} = \frac{GMm_{\rm H}}{r^2}, \tag{1.49}$$

where $m_{\rm H}$ is the hydrogen mass.

By equating the radiation-pressure force and the gravitational force, we obtain Eddington luminosity $L_{\rm E}$

$$L_{\rm E} = \frac{4\pi cGMm_{\rm H}}{\sigma_{\rm T}}. \tag{1.50}$$

Eddington luminosity does not depend on r. A non-rotating spherical object with mass M cannot shine with luminosity greater than the Eddington luminosity $L_{\rm E}$.

In case of accretion disks the critical mass-accretion rate associated with the Eddinggton luminosity is defined as

$$\dot{M}_{\rm crit} \equiv \frac{L_{\rm E}}{c^2}, \tag{1.51}$$

however, because accretion disks are rotating, they can exceed the Eddington limit, but can no longer be modeled in a thin approximation.

1.4.2 Observed spectrum

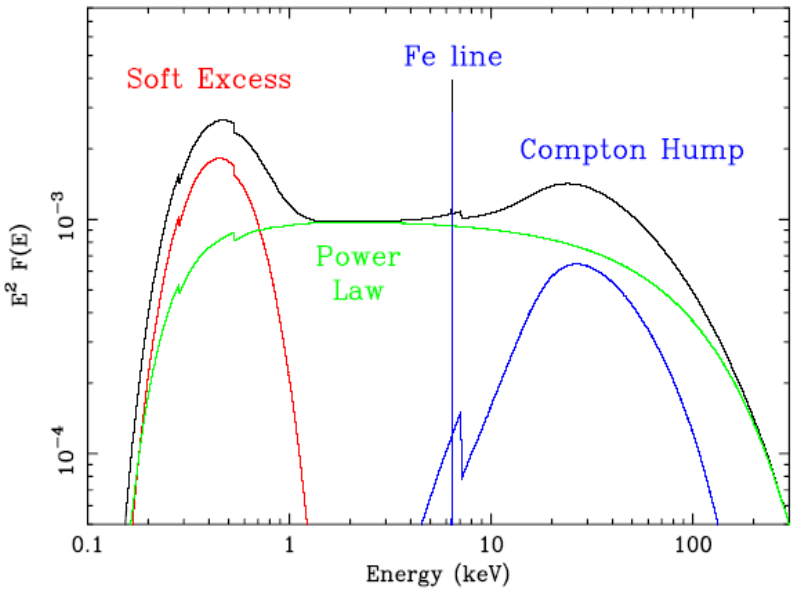

Figure 1.3: The main components of X-ray spectra: soft X-ray emission from the accretion disk(red); power law from Comptonization of the soft X-rays in corona above the disk (green); reflection continuum and narrow Fe line due to reflection of the hard X-ray emission from dense gas (blue), summarized spectrum (black), (Fabian, 2006).

As we have established above, disk spectrum is represented by a multi-colored black body spectrum. In a typical AGN that host a supermassive black hole of the mass of several millions solar masses, the inner regions of an accretion disk, where most of the energy is released, radiate in the ultraviolet and marginally in soft X-ray bands. Outer regions, where least of the energy is released, radiate in the optical band. Radiation spectra of the disk are formed locally at the effective photosphere and the shape of the spectrum depends on the distance to the central object (black hole).

X-rays observed from AGN are usually explained by an inverse Compton emmision of thermal radiation in a hot matter called *corona*. Corona is assumed to be above an accretion disk and mainly consists of hot electrons. Outgoing spectra have strong dependence on parameters of corona, e.g. temperature of electrons in corona, geometry of corona (see figure 1.7), its optical depth (see figure 1.8) etc. Exemplary outgoing spectra are shown in figures 1.3 and 1.4. From these figures one can see, that observed spectra can be very diffent.

Accretion disk produces thermal photons that are scattered to all directions by corona. A certain part of photons can also be back-scattered to an accretion disk, and then be either reflected by the disk, or absorbed by it as it is shown in figure 1.5. Probability of a photon be either reflected, or absorbed depends on its energy boost after comtonization in corona and on the properties of the disk, e.s. its ionization. Absorbed photons will be in further thermally reradiated by an accretion disk. Reflected photons can be then observed, and assumed to be responsible for the formation of Compton hump and Fe line in the observed

spectra (see figures 1.3, 1.4).

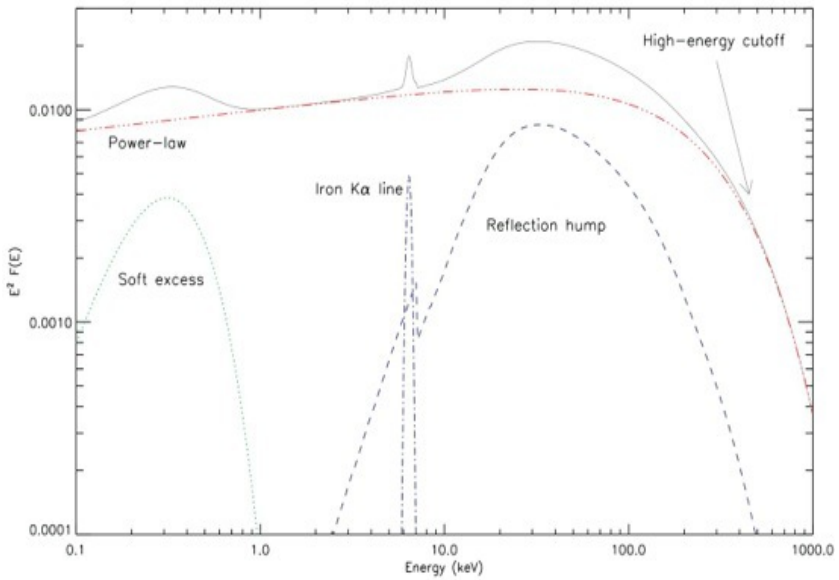

Figure 1.4: Example of possible observed spectrum from AGN.

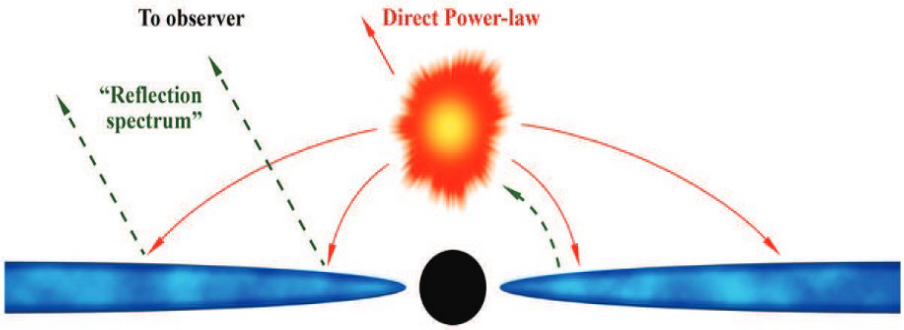

Figure 1.5: Formation of power law component and the reflection component of the spectrum.

In order to understand observed spectra from AGN, it is important to consider Comptonization in corona more specifically. Black hole's corona consists of hot electrons, non-thermal distribution of electrons is set by electron temperature $\Theta = kT_e/m_ec^2$. The number of photons is conserved during Comptonization and the probability a photon will meet an electron can be calculated from the optical depth τ of corona. Probability that a photon will be scattered by an electron is given by $1 - e^{-\tau}$. Photons in the corona can be scattered on electrons multiple times which is shown in figure 1.6. Spectrum built up from multiple Compton scattering is usually approximated with power law function(green solid line in figure 1.6) with power law index $\alpha = \ln\tau/\ln(1+4\Theta)$. Note that the power law index is determined by both the temperature and the optical depth of the electrons.

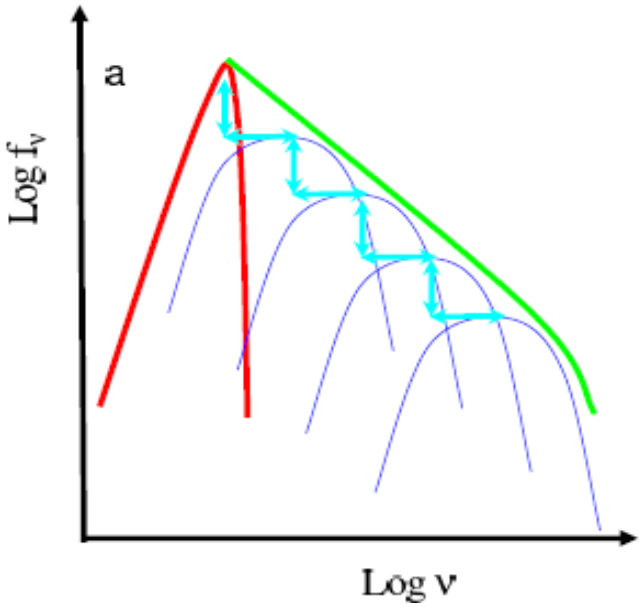

Figure 1.6: Spectrum built up from multiple Compton scaterring for optically thin ($\tau < 1$) material. Fraction $1 - e^{-\tau}$ of thermal low energy photons boosted in energy by Compton scatrring is denoted by red solid line, each next scaterring order is denoted by blue solid line, approximation with power law is denoted by green solid line, shift factor of scaterring orders is denoted by cyan arrows (Done, 2010).

As one can see from figure 1.3, a typical X-ray spectrum from AGN is composed of three main components, where two of them were commented above (blue line and green line), and a soft excess (red line). In contrast with power law component and reflection component (Compton hump and Fe line), there is much greater uncertainty in origin of the soft excess. According to one of many hypotheses it can be partially thermal radiation of the disk and partially own (free-free) radiation of the corona. But there is still no exact explanation to the nature of the soft excess line.

Power law part of the above spectrum can have different forms (see figures 1.3, 1.4), its slope can be either positive or negative and, in general, is source-dependent. Spectra from AGN can be drawn with different system of axes, it is normally drawn with $F_\nu(\nu)$-axes, but for visibility reasons it can be drawn with $\nu F_\nu(\nu)$-axes or with $\nu^2 F(E)$-axes, as it is in figires 1.3, 1.4 . In case of spectrum is drawn with $F_\nu(\nu)$, its power law index is defined by α, but when spectrum is drawn with $\nu F_\nu(\nu)$-axes, its power law index is defined by Γ, and is then called *photon index*. Photon index is defined as $\Gamma = \alpha + 1$ and is of typical values $\Gamma \sim 1.5 - 3.5$ (e.g. Nandra and Pounds, 1994; Reeves and Turner, 2000).

X-ray spectra are commonly analyzed with the help of spectral fitting package XSPEC, which was firstly written in 1983 at the Institute of Astronomy, Cambridge, under VAX/VMS by Rick Shafer. XSPEC was meant to perform spectral analysis of data from the ESA EXOSAT X-ray observatory. By now XSPEC represents the main powerful tool in spectral analysis of AGN. XSPEC package includes number of different physical models which can be applied to different astrophysical objects and simulate outgoing spectra.

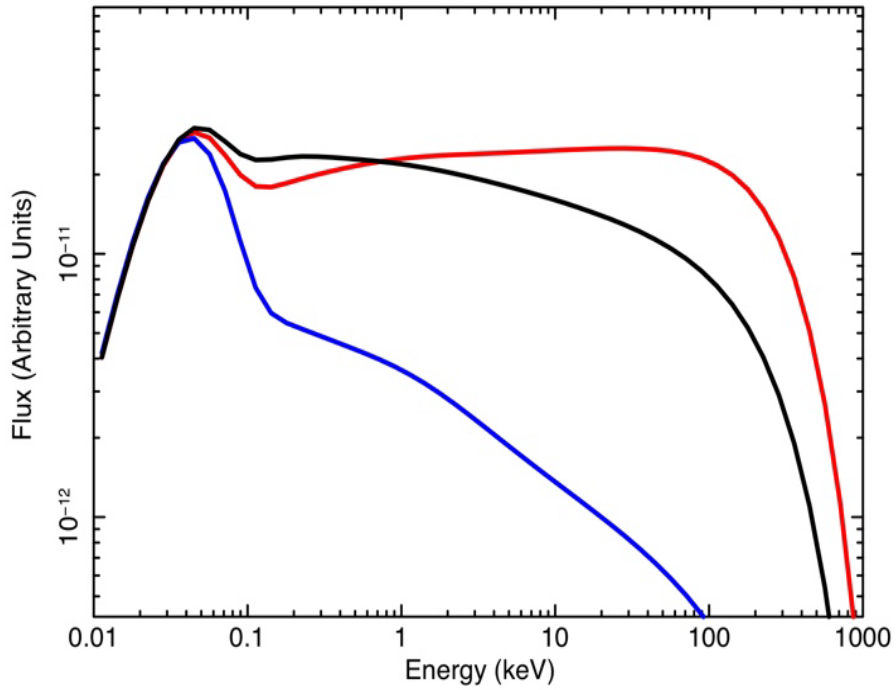

Figure 1.7: Observed spectra depending on the corona geometry: slab geometry (red), cylinder corona (blue), spherical corona (black), (Malzac, 2018)

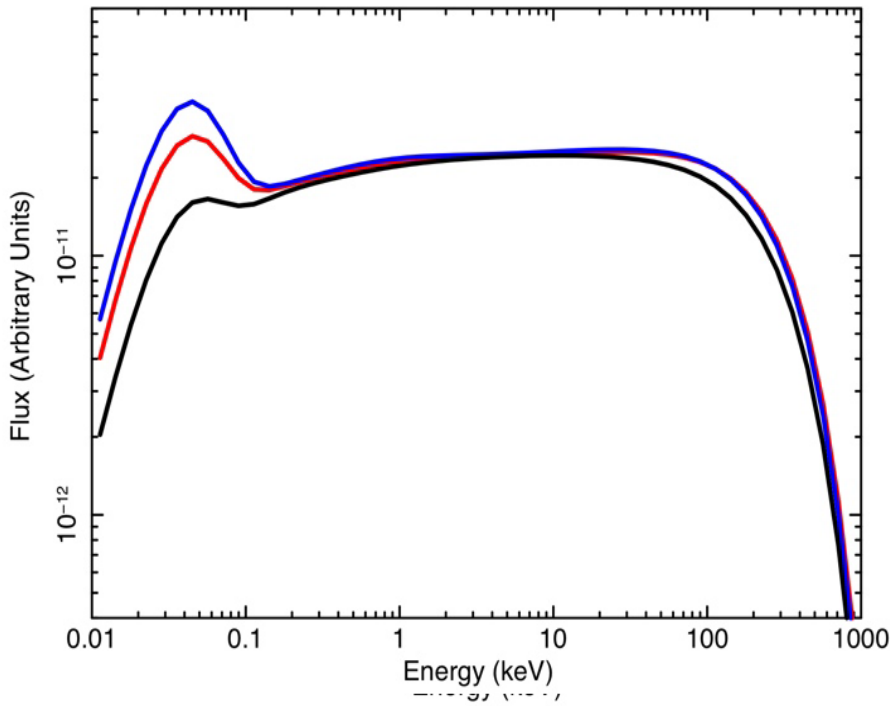

Figure 1.8: Observed spectra depending on the optical depth τ of the corona: $\tau = 0.5$ (red), $\tau = 1$ (blue), $\tau = 0.7$(black), (Malzac, 2018)

Black-hole corona

2.1 Possible configurations of corona

The existence and origin of AGN corona is still a puzzle in astrophysics, nevertheless, there are few hypotheses. The simpliest model is 'lamppost' model (see figure 2.1) that assumes the corona to be a point-like source located at a certain height above the black hole. 'Lamppost' model can be treated either classically (non-relativistically) or fully relativistically, and even in fully relativistic approach it doesn't correlate with observations (Dovciak and Done, 2015). Thereby, 'lamppost' model does not seem to be the true physical explanation.

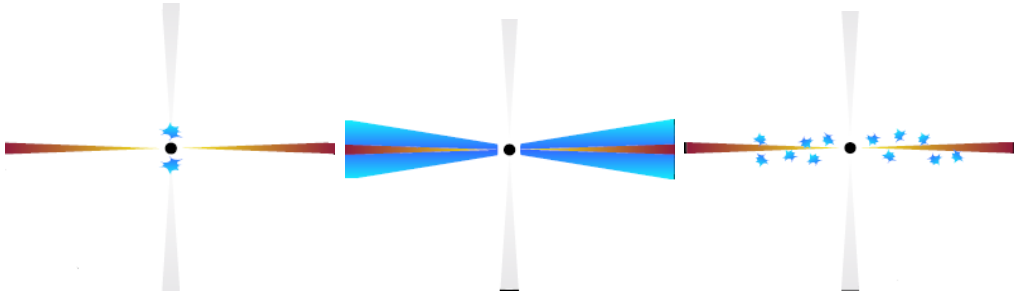

Figure 2.1: Left panel: 'lamppost' corona, middle panel: 'sandwich' gometry of corona, right panel: 'patchy' geometry of corona (Malzac, 2018).

Another model is called the 'sandwich' model (see figure 2.1). 'Sandwich' model assumes the corona to be a layer above an accretion disk covering the whole surface of the disk. This layer could be treated either as if it was straight above the disk or at a height h above it that will only complicate the calculations, thus, it is more convenient to consider corona be right above the disk. In Haardt and Maraschi (1991) was developed a two-phase accretion disk model with 'sandwich'-like corona, where authors composed and solved balance equations between corona and black hole accretion disk. Their solutions of global equations yield the temperature of corona being a function of its optical depth τ. Hereafter, Haardt et al. (1994) after further research, concluded that corona may have a patchy structure. Therefore, another possible configuration of corona appears, and it is plain patchy corona above an accretion disk (see figure 2.1).

Corona can also be considerd cloud-like (see figure 2.2). In this case black-hole corona supposed to be concentrated above a certain place of an accretion disk, and not covering its whole surface. There are several other possibilities for geometry of the corona, such as jet-like corona (see figure 2.2), spherical or cylinder corona (see figure 2.3). In this thesis we will further focus on sandwich model of the corona and show what are geometrical constraints based on energy conservation considerations.

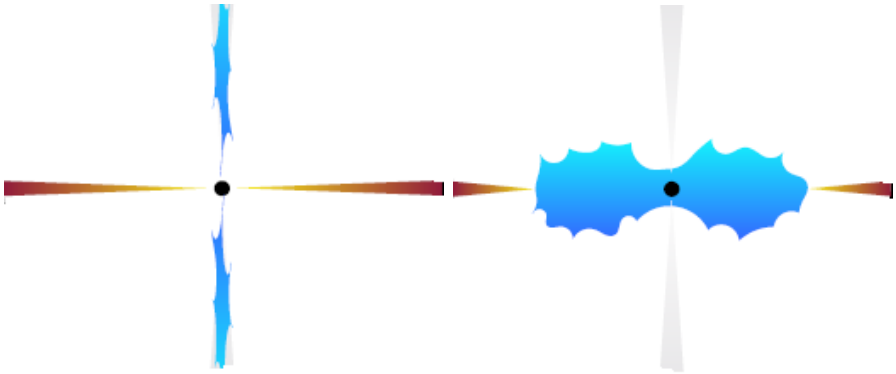

Figure 2.2: Left panel: jet-like corona, right panel: cloud-like corona (Malzac, 2018).

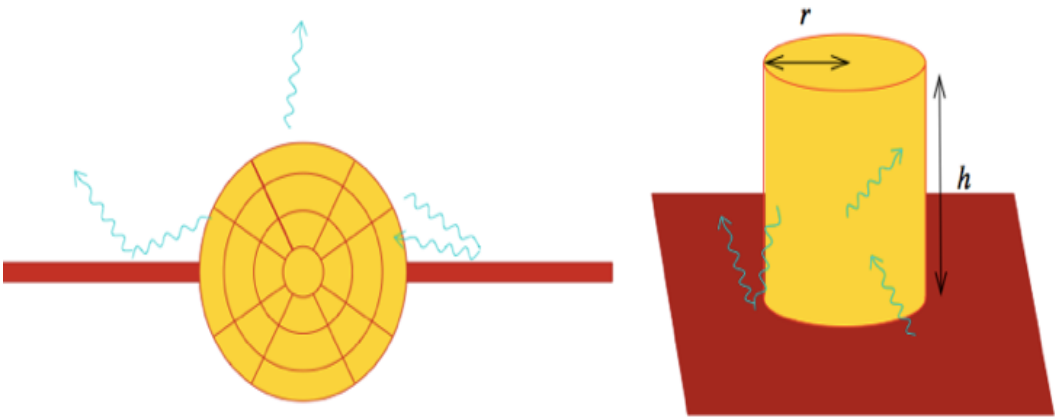

Figure 2.3: Cylinder and sperical geometries of corona (Stern et al., 1995); (Poutanen and Svensson, 1996).

2.2 Energy balance of 'sandwich'-like corona

Let us first define some values that we will widely use in this and in the following sections. *Specific intensity* dI_ν is defined as a finite amount of energy dE transported by radiation of frequences $(\nu, \nu + d\nu)$ emitted from an area dA that is seen at a solid angle $d\Omega$ in a small duration of time dt. Thus,

$$dI_\nu = \frac{dE}{dt\ dA\ d\nu\ d\Omega}. \tag{2.1}$$

Specific flux can be defined as a finite amount of energy dE transported by radiation of frequences $(\nu, \nu + d\nu)$ emitted from an area dA in a small time duration dt

$$dF_\nu = \frac{dE}{dt\ dA\ d\nu}, \tag{2.2}$$

and with the help of specific intensity is $F_\nu = \int I_\nu d\Omega$, see also (1.34). *Flux* can be defined with the help of *specific flux*, and is

$$F = \int F_\nu d\nu. \tag{2.3}$$

Specific photon flux can be defined from specific flux as follows

$$dN_\nu = \frac{dF_\nu}{h\nu} = \frac{dN}{dt\ dA\ d\nu} = h\frac{dN}{dt\ dA\ dE}, \tag{2.4}$$

where $dE = hd\nu$.

At the first step we consider a two-phase accretion disk with a 'sandwich' corona lying straight above an accretion disk and covering its whole surface. A picture of the model that we use is shown in figure 2.4. As we examined before, accretion disk radiates as a black body with an effective temperature $T^{\rm eff}_{\rm DISK}$, and its flux is thus given by $F = \sigma T^{\rm eff}_{\rm DISK}$. Nevertheless, we will assume a certain part of the energy that comes from accretion process retreats to magnetic fields which carry that energy to corona and energize coronal electrons. Let us denote energy from accretion process by $L_{\rm ACC}$ (energy balance will be composed in terms of radiative energy per unit time), energy radiated out from the disk surface as a black body spectrum by $L_{\rm DISK}$, and energy carried by magnetic fields to heat corona by $L_{\rm SC}$. The total energy that escapes from the system is $L_{\rm OUT}$ and obviously it must be equal to $L_{\rm ACC}$, if the total energy is to be conserved.

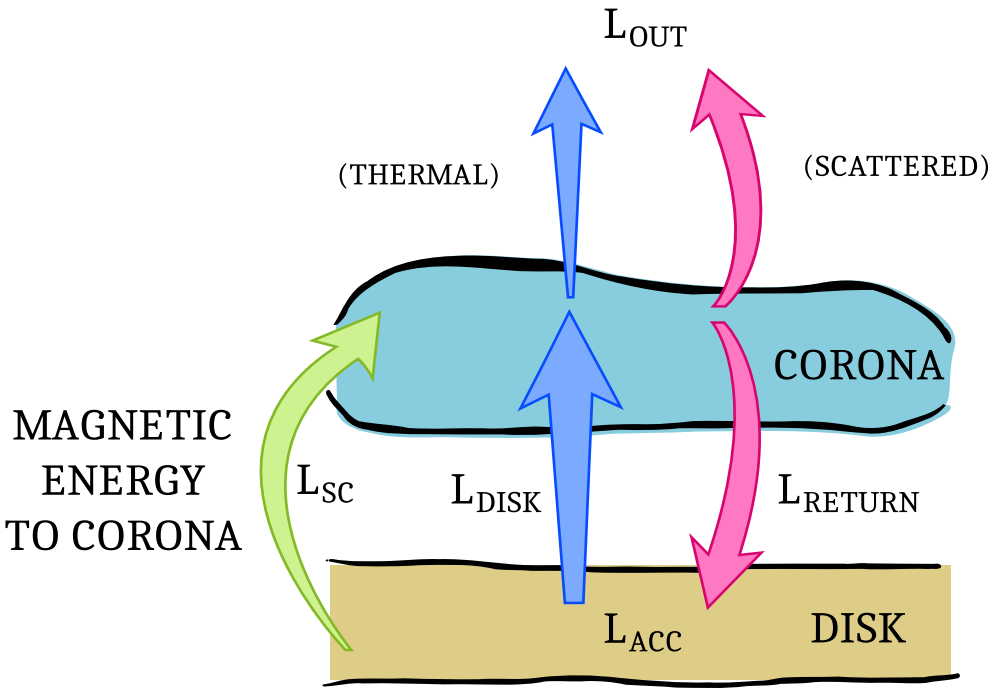

Figure 2.4: Energy produced by an accretion process $L_{\rm ACC}$ is shared between the thermal energy $L_{\rm DISK}$ and the energy of magnetic fields $L_{\rm SC}$. Thermal part of the accretion energy $L_{\rm DISK}$ is radiated by the disk as a black body spectrum, and then can be either scattered by corona, or pass the corona unscattered. A certain part of thermal energy $L_{\rm DISK}$ can be backscattered to the disk $L_{\rm RETURN}$ and contribute to the local energy balance in the disk. The energy of magnetic fields $L_{\rm SC}$ energizes electrons in the corona.

Photons radiated as a black body are further partially scattered by corona and partially let go through the corona without an interaction (see arrows 'thermal' and 'scattered' in figure 2.4). A certain part of scattered photons is assumed to be

backscattred to an accretion disk (see arrow L_{RETURN} in figure 2.4), because the process of Compton scattering is not angle-dependent (at low electron temperatures). Let us denote back-scattered energy by L_{RETURN}. This back-scattered energy is assumed to be fully thermalized in the disk and contributs to its local energy balance, i.e. affects its effectiv temperature.

Thus, we can compose energy balance equations between the accretion disk and the slab corona considering energy conservation

$$L_{\mathrm{OUT}} = e^{-\tau} L_{\mathrm{DISK}} + \frac{1}{2}\left[(1 - e^{-\tau}) L_{\mathrm{DISK}} + L_{\mathrm{SC}}\right], \tag{2.5}$$

$$L_{\mathrm{RETURN}} = \frac{1}{2}\left[(1 - e^{-\tau}) L_{\mathrm{DISK}} + L_{\mathrm{SC}}\right], \tag{2.6}$$

$$\begin{cases} (\text{radiative cooling}) : L_{\mathrm{RAD}} = \alpha L_{\mathrm{ACC}} \\ (\text{magnetic fields}) : L_{\mathrm{SC}} = (1 - \alpha) L_{\mathrm{ACC}}, \end{cases} \tag{2.7}$$

$$L_{\mathrm{DISK}} = L_{\mathrm{RAD}} + L_{\mathrm{RETURN}}, \tag{2.8}$$

$$\begin{gathered} L_{\mathrm{OUT}} = L_{\mathrm{ACC}} \\ (\text{energy conservation}), \end{gathered} \tag{2.9}$$

where energy given by accretion process L_{ACC} is shared between magnetic fields L_{SC} and thermal radiation L_{RAD} by a parameter $\alpha \in [0,1]$ (see also Haardt et al., 1994). If we adopt $\alpha = 1$, all the accretion energy will be thermally radiated and there will be no energy carried by magnetic fields, or vice versa, in the limit $\alpha = 0$, zero energy is radiated thermally, and all the accretion energy is carried by magnetic fields. In order to obtain outgoing spectrum, it is necessary to determine a parameter α so all the equations (2.5) - (2.9) hold.

In order to solve equations (2.5) - (2.9), we wrote a numerical simulation that computes parameter α. In our simulation we use NTHCOMP from XSPEC package, to model the black body spectrum after passing through the corona. NTHCOMP model simulates the Compton process in the corona using the model of thermally comptonized continuum (Zdziarski et al., 1996; Zycki et al., 1999). Free parameters for NTHCOMP are the black body temperature $T^{\mathrm{eff}}_{\mathrm{DISK}}$, photon index Γ and temperature of electrons in the corona T_e. In our simulation NTHCOMP model calculates two parts of the incident thermall radiation that meets the corona, one that is scattered by the corona and the other that passes through the corona unscattered (see arrows 'thermal'(blue) and 'scattered'(red) in figure 2.4). Optical depth τ of the corona is calculated from equation (A1) from (Zdziarski et al., 1996).

Simulation was tested with different initial parameters Γ and T_e. For a black hole with the mass $M = 10^7 M_\odot$ simulation stopped working at paramaters $\Gamma < 2.5$ (see figure 2.7), $T_e = 30$keV, where for those parametrs there was no solution for α. From a physical point of view this result means that cold accretion disk cannot produce enough amount of power to keep coronal electrons energized. For example, for the set of parameters $\Gamma = 3.0$, $T_e = 30$keV, $M = 10^7 M_\odot$ we obtain a local spectrum which is shown in figure 2.5. In figure 2.5 one can see a part forming a black body spectrum and parts converging to power law, which

resembles the general shape of an AGN spectrum except for soft excess and Compton hump that we neglect in our simulation for simplicity reasons. Thus, slab corona geometry with full coverage can be applied only to corona with steep photon index $\Gamma \geq 2.5$ which does not correlate well with observations that support rather hot corona with often not so steep photon indices. This demonstrates that a slab model of corona with full coverage is not a suitable description of the real AGN corona. It invokes us to consider a slightly more general configuration of corona's geometry.

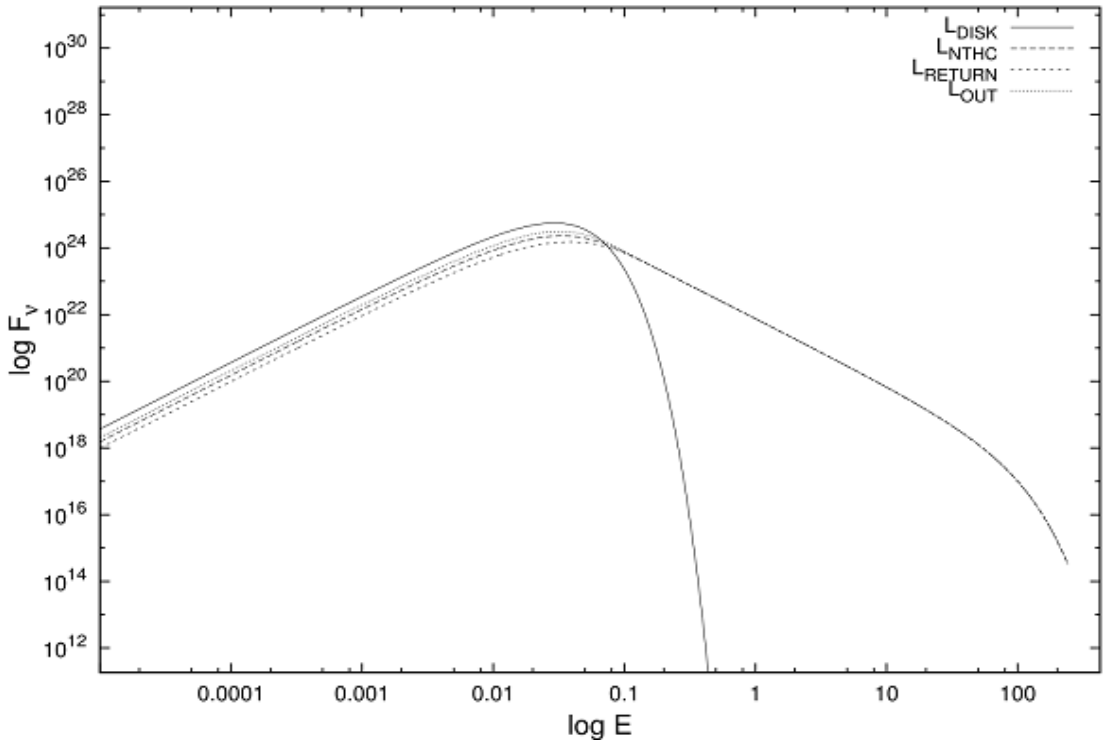

Figure 2.5: Outgoing local spectrum of an accretion disk with the mass of the black hole $M = 10^7 M_\odot$ and black-hole spin $a = 0$ and parameters $\Gamma = 3$, $T_e =$ 30keV of corona. The spectrum is evaluated at radius $r = 10$rg. Solid line corresponds to thermal black body radiation from the disk, small dots denote observed spectrum L_{OUT}, short-dashed line denoted photons back-scattered by the corona L_{RETURN}, long-dashed line denotes part simulated by NTHCOMP L_{NTHCOMP}.

2.3 Energy balance of patchy corona

Another possible configuration of corona that we can consider is a patchy corona. Thus, it becomes necessary to define a covering factor k of corona, $k \in [0, 1]$. The factor k can be either related to geometry of corona, thereby, it describes the percentage of the disk surface that is covered by corona, or this factor can be treated as time-factor of the magnetic fields which means that electrons in the corona will be energized occasionally after a sufficient amount of energy is accumulated in the magnetic fields. In further we will treat factor k as a covering

factor that controls abundance of the corona above the accretion disk.

In the patchy configuration the corona is still covering all the radii of an accretion disk but it is no longer a solid layer, but has "holes" in it. Now we should rewrite energy balance equations (2.5) - (2.9) with covering factor k participating. Energy balance equations for patchy corona, thus, become

$$L_{\text{DISK}} = L_{\text{RAD}} + L_{\text{RETURN}}, \tag{2.10}$$

$$L_{\text{OUT}} = (1-k)L_{\text{DISK}} + ke^{-\tau}L_{\text{DISK}} + \frac{1}{2}k(1-e^{-\tau})L_{\text{DISK}} + \frac{1}{2}L_{\text{SC}}, \tag{2.11}$$

$$L_{\text{RETURN}} = \frac{1}{2}k(1-e^{-\tau})L_{\text{DISK}} + \frac{1}{2}L_{\text{SC}}, \tag{2.12}$$

$$\begin{cases} L_{\text{RAD}} = \alpha L_{\text{ACC}} \\ L_{\text{SC}} = (1-\alpha)L_{\text{ACC}}, \end{cases} \tag{2.13}$$

$$L_{\text{OUT}} = L_{\text{ACC}}, \tag{2.14}$$

where in equation (2.11) term $(1-k)L_{\text{DISK}}$ denotes a certain part of photons that will not meet the corona and pass through its "holes" . This part will contribute to the black body spectrum.

Using equations (2.13) we obtain

$$L_{\text{DISK}} = \alpha L_{\text{ACC}} + L_{\text{RETURN}}, \tag{2.15}$$

$$L_{\text{RETURN}} = \frac{1}{2}k(1-e^{-\tau})L_{\text{DISK}} + \frac{1}{2}(1-\alpha)L_{\text{ACC}}, \tag{2.16}$$

$$L_{\text{OUT}} = \left[(1-k) + ke^{-\tau} + \frac{1}{2}k(1-e^{-\tau})\right]L_{\text{DISK}} + \frac{1}{2}(1-\alpha)L_{\text{ACC}}. \tag{2.17}$$

Expressing L_{RETURN} from equation (2.10) and substituing it to equation (2.16) we obtian

$$L_{\text{DISK}} - \alpha L_{\text{ACC}} = \frac{1}{2}k(1-e^{-\tau})L_{\text{DISK}} + \frac{1}{2}(1-\alpha)L_{\text{ACC}}. \tag{2.18}$$

Hence, from (2.18) we obtain

$$\frac{L_{\text{DISK}}}{L_{\text{ACC}}} = \frac{\alpha+1}{2-k(1-e^{-\tau})}, \quad \alpha \in [0,1]. \tag{2.19}$$

Since $\alpha \in [0,1]$ and $k \in [0,1]$, then

$$\gamma < \frac{L_{\text{DISK}}}{L_{\text{ACC}}} < 2\gamma\ , \tag{2.20}$$

where

$$\gamma = \frac{1}{2-k(1-e^{-\tau})}, \ \ \gamma \in [\frac{1}{2}, 1]$$

.

Using NTHCOMP model we can modify our energy balance equations as follows

$$L_{\rm OUT} = (\text{black body}) + (\text{NTHCOMP})\,, \tag{2.21}$$

$$L_{\rm NTHCOMP}(T^{\rm eff}_{\rm DISK}, \Gamma, T_e) = \frac{1}{2}k(1-e^{-\tau})L_{\rm DISK} + \frac{1}{2}L_{\rm SC} + \frac{1}{2}ke^{-\tau}L_{\rm DISK}. \tag{2.22}$$

Equation (2.22) follows from the geometry of corona that is considered in NTHCOMP model. Originally, NTHCOMP assumes corona to be spherical, where a half of the scattered thermal radiation escapes from the corona to the observer, and other half is back-scattered to the opposite side. In our model we assume corona to be a plain layer above the disk, so we modified the normalization of NTHCOMP model so to correspond to the slab geometry of corona in a way used in equation (2.22). Hence

$$L_{\rm OUT} = (1-k)L_{\rm DISK} + ke^{-\tau}L_{\rm DISK} + \frac{1}{2}\left[k(1-e^{-\tau})L_{\rm DISK} + L_{\rm SC}\right]. \tag{2.23}$$

Using (2.22) we obtain

$$L_{\rm OUT} = \left[1 - k + \frac{1}{2}ke^{-\tau}\right]L_{\rm DISK} + L_{\rm NTHCOMP}(T^{\rm eff}_{\rm DISK}, \Gamma, T_e). \tag{2.24}$$

For the above mentioned geometrical reasons we set the normalization for the number of photons in NTHCOMP model as

$$N_{\rm NTHCOMP} = \frac{1}{2}kN_{\rm DISK}. \tag{2.25}$$

Photon distribution of a black body whose radiation is given by Planck's law

$$F_\nu = \frac{2\pi h\nu^3}{c^2}\frac{1}{e^{h\nu/kT}-1}$$

can be calculated as follows

$$\begin{gathered} N = \frac{1}{c^2}\int_0^\infty \frac{\nu^2}{e^{h\nu/kT}-1}\,d\nu = \frac{1}{c^2}\int_0^\infty \frac{\left(\frac{xkT}{h}\right)^2\frac{kT}{h}}{e^x-1}\,dx = \\ = \frac{(kT)^3}{c^2h^3}\int_0^\infty \frac{x^2e^{-x}}{1-e^{-x}}dx = \\ = \frac{(kT)^3}{c^2h^3}\int_0^\infty x^2e^{-x}(1+e^{-x}+e^{-2x}+...)\,dx = \left[\int_0^\infty x^ne^{-ax}dx = \frac{n!}{a^{n+1}}\right] = \\ = \frac{(kT)^3}{c^2h^3}\,4\cdot(1+\frac{1}{2^3}+\frac{1}{3^3}+...) = \sigma_pT^3, \end{gathered} \tag{2.26}$$

where $\sigma_p = \frac{4k^3T^3\zeta(3)}{c^2h^3}$ is photon Stefan-Boltzmann konstant, $\zeta(s) = \sum_{n=1}^\infty \frac{1}{n^s}$ is Riemann zeta function.

Thus,

$$N_{\rm DISK} = \sigma_p(T^{\rm eff}_{\rm DISK})^3, \tag{2.27}$$

and from equation (2.25) we have

$$N_{\mathrm{NTHCOMP}} = \frac{1}{2} k \sigma_p (T^{\mathrm{eff}}_{\mathrm{DISK}})^3. \tag{2.28}$$

Equation (2.24) can be written in terms of specific flux, which gives us the expected emerging spectrum

$$F_\nu^{\mathrm{OUT}} = F_\nu^{\mathrm{BB}} \left(T^{\mathrm{eff}}_{\mathrm{DISK}}\right) (1 - k + \frac{1}{2} k e^{-\tau}) + F_\nu^{\mathrm{NTHCOMP}}(\Gamma, T_e, T^{\mathrm{eff}}_{\mathrm{DISK}}), \tag{2.29}$$

where we have the same two components as in the energy equation (2.24). The thermal part is represented by a black-body spectrum F_ν^{BB} and the comptonized part plus a fraction of thermal radiation that is unscattered in the corona is represented by F_ν^{NTHCOMP}. The later is obtained as an output of the XSPEC NTHCOMP model.

Technically, our model now has two free parameters, which are the covering factor k of corona and the factor α that divides energy between thermal radiation and magnetic fields. These two parameters, however, depend on each other and fixing one directly determines the value of the other one. Hence, it is more convenient to have an analytical equation for one as a function of another one, e.g. for the parameter k. In order to derive an analytical equation for the parameter k, we define average photon energies for the NTHCOMP part of the spectrum and for the thermal part as follows

$$\bar{E}_{\mathrm{NTHCOMP}} = \frac{L_{\mathrm{NTHCOMP}}}{N_{\mathrm{NTHCOMP}}} = \frac{L_{\mathrm{NTHCOMP}}}{\frac{1}{2} k \sigma_p (T^{\mathrm{eff}}_{\mathrm{DISK}})^3}, \tag{2.30}$$

$$\bar{E}_{\mathrm{DISK}} = \frac{L_{\mathrm{DISK}}}{N_{\mathrm{DISK}}} = \frac{L_{\mathrm{DISK}}}{\sigma_p (T^{\mathrm{eff}}_{\mathrm{DISK}})^3}. \tag{2.31}$$

Thus, we can define a new parameter ϵ as a ratio between average energies $\bar{E}_{\mathrm{NTHCOMP}}$ and $\bar{E}_{\mathrm{DISK}}$

$$\epsilon = \frac{\bar{E}_{\mathrm{NTHCOMP}}}{\bar{E}_{\mathrm{DISK}}} = \frac{2}{k} \frac{L_{\mathrm{NTHCOMP}}}{L_{\mathrm{DISK}}}. \tag{2.32}$$

From equations (2.22), (2.24) we can derive

$$\frac{L_{\mathrm{OUT}}}{L_{\mathrm{DISK}}} = 1 - k + \frac{1}{2} k (\epsilon + e^{-\tau}) = \frac{2 - k(1 - e^{-\tau})}{1 + \alpha}. \tag{2.33}$$

Hence, for the parameter k it holds

$$k = \frac{2(1 - \alpha)}{\alpha(\epsilon + e^{-\tau}) + (\epsilon - e^{-\tau}) + 2\alpha}. \tag{2.34}$$

From equation (2.34) follows boundary condition for k, and is given by

$$k \leq \frac{2}{\epsilon - e^{-\tau}}, \;\; \epsilon > 1. \tag{2.35}$$

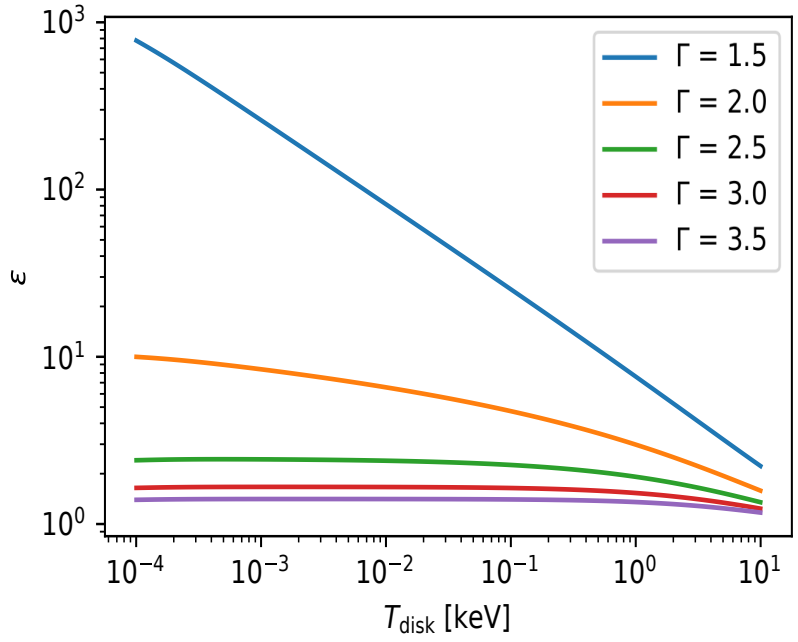

Figure 2.6: Dependence of the paramter ϵ on the temperature of the disk T_{disk} for the different values of Γ and for $T_e = 50$keV.

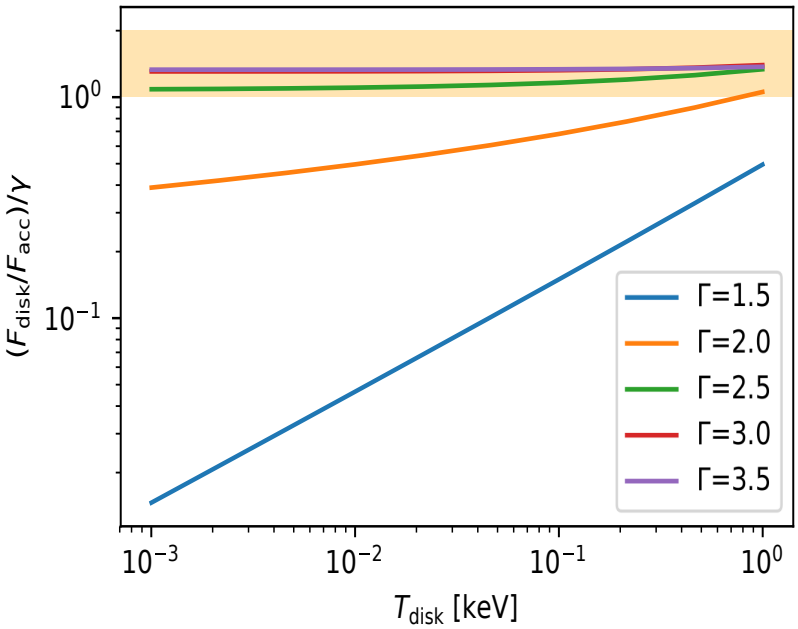

Figure 2.7: The range of allowed solutions for the equation set (2.10) - (2.14) for different values of Γ ($T_e = 50$keV). The yellow box shows the allowed range for the value of the coverage factor $k = 1$, where only coronae with steep Γ fit. Lowering k will lower the position of the allowed region in the plot along y-axis.

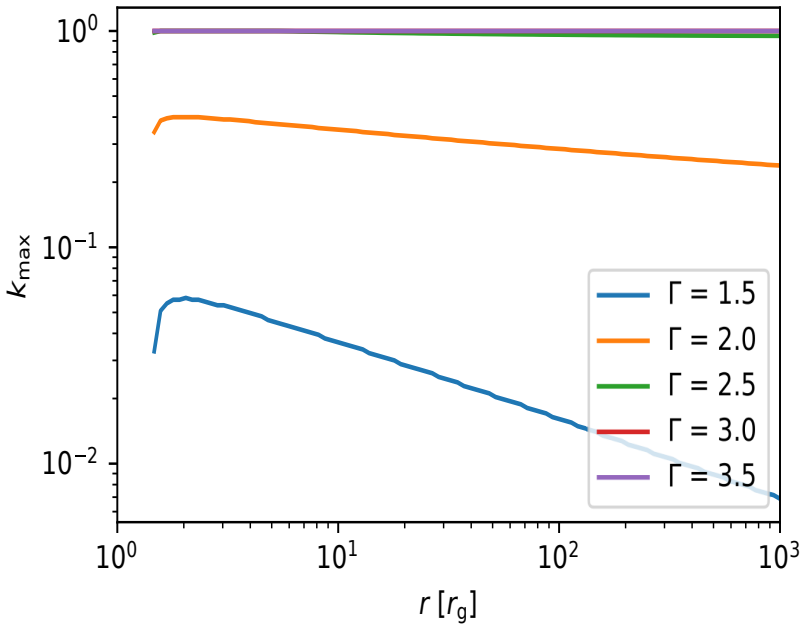

Figure 2.8: Dependence of the maximal value of the parameter k on the radius of the accretion disk r with the black-hole mass $M = 10^7 M_\odot$, black-hole spin $a = 0,999$ and temperature of the electrons in the corona $T_e = 50$keV for different photon indices.

Parameter ϵ can be also very useful if we draw it depending on the temperature of the accretion disk for the different values of the photon index Γ. One can see that for the steep photon indices (see figure 2.6) there is a minimal difference between thermally radiated energy and the comptonized fraction, thus, after comptonization in the corona, observed spectra will be more influenced by the black body spectrum than by power law. On the other hand, the difference between energies radiated by the disk and comptonized fraction becomes clearer with decreasing photon index Γ, in this case the observed spectrum will be more dominated by power law than by the black body spectrum.

We can use relation (2.20) to show what is the range of allowed solutions of the energy equations (2.10)-(2.14) based on the model parameters Γ, T_e and k. Figure 2.7 shows how relation (2.20) depends on the black-body effective temperature T_{DISK} and on Γ index (electron temperature T_e is fixed at 50 keV) and what is the range of solutions for a fixed value of the coverage factor k – in the depicted case $k = 100\%$. Clearly, a corona that fully covers the disk can only exist if it has sufficiently steep photon index ($\Gamma > 2.5$). Coronae with lower Γ must necessarily be patchy to meet the condition on the energy balance. In the plot it means that the coverage factor will be lower and the yellow box will also move lower along the vertical axis. This means simply that an optically thicker corona with low value of Γ must have holes to allow a significant fraction of thermal photons to pass without interactions, otherwise those photons would cool the corona beyond the ability of the disk to cover the energy losses from its internal accretion energy.

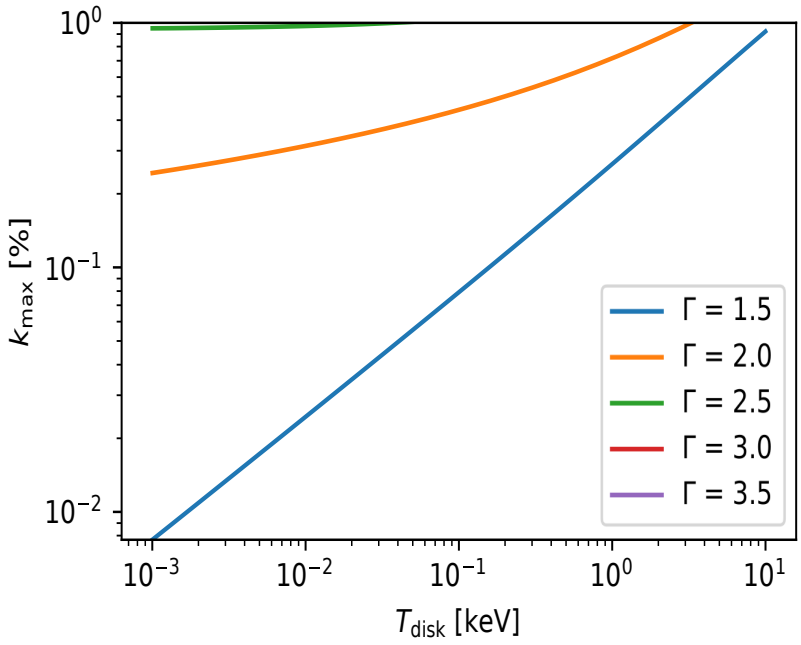

Figure 2.9: Dependence of the maximal allowed value of the parameter $k_{\max}$ on the effective temperature of the accretion disk T_{disk} for different photon indices Γ.

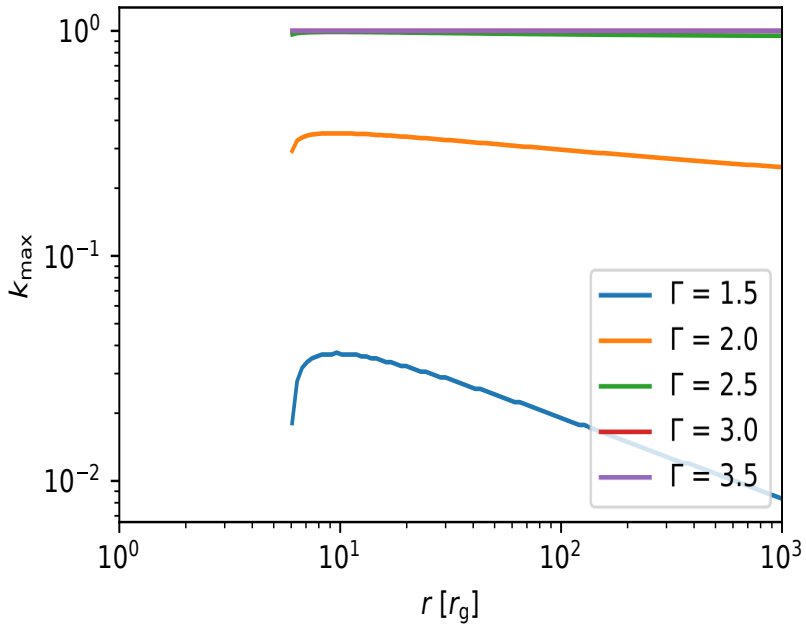

Figure 2.10: Dependence of the maximal value of the parameter k on the radius of the accretion disk r with the black-hole mass $M = 10^7 M_\odot$, black-hole spin $a = 0$ and temperature of the electrons in the corona $T_e = 50$keV for different photon indices.

The fact, that the effective temperature of the accretion disk depends on radius, and since equation (2.35) constrains the maximal value of the parameter k, the set of graphs of $k_{\max}(T_{\rm disk})$ and $k_{\max}(r)$ give us the maximal allowed coverage factor of the corona above the accretion disk. Abundance of the corona above the accretion disk for the black hole with the mass $M = 10^7 M_\odot$ and black hole spins $a = 0$, $a = 0,999$ can be seen from the set of figures (2.8), (2.9), (2.10).

2.4 Outgoing spectra from the accretion disk with 'patchy' corona

Up until now, we have been only dealing with the local spectra, i.e. the spectra of radiation emerging from corona locally in the rest frame of the rotating fluid at a specific radius. In order to obtain the global spectrum of accretion disk, we need to integrate that local spectra over the surface of the accretion disk. Because we are dealing with disks around compact object, that integration shall treat all the relativistic effects that affect the photons on the way to a distant observer. These are namely the Doppler boosting, beaming and gravitational light bending and red-shift.

We are using an integration scheme, where the local intensity is integrated over the disk surface with the use of a transfer function that incorporates all the relativistic effects and transformations. A general formula for such an integration in terms of photon flux is

$$N_{\rm obs}(E) = \int N_{loc}(E/g)\, g^2\, d\Omega\,, \tag{2.36}$$

where $N_{\rm obs}(E)$ is the specific photon flux as seen by the observer, $N_{\rm loc}(E)$ is the specific photon flux emitted from the fluid rest frame, g is the relativistic red-shift factor combining Doppler effect and gravitational red-shift and $d\Omega$ is an element of the solid angle on the observer's sky. Since we have decided to integrate over the disk surface rather that over the observer's sky, we need to transform $d\Omega$ to a disk surface element $r\, dr\, d\varphi$. Then

$$N_{\rm obs}(E) = N_0 \int\int N_{loc}(E/g)\, F(r, g, \mu_{\rm e})\, r\, dr\, d\varphi\,, \tag{2.37}$$

where N_0 is normalization and $F(r, g, \mu_{\rm e})$ is a transfer function that depends on the place and direction of emission and $N_{loc}(E/g)$ is the local photon spectrum that corresponds to equation (2.24).

This integration framework has been used by Dovciak et al. (2004) to develop a set of spectral models for the fitting software XSPEC. The so called KY models are frequently used in analysis of observed AGN data and we use one of the models (KYNBB, the disk thermal emission model) as a basis for deriving a new spectral model that will implement the local spectra of radiation that comes from the sandwiched corona as describes in Section 2.2.

We name the new model KYNCOMP and the source files for it are attached to the thesis. Although the model is based in non-axisymmetric integration routine from the KY core (which is indicated by the letter N in the name), the routine that implements the local spectrum is of course axially symmetric with no azimuthal

angle dependence. The non-axisymmetric feature may be, however, used later in a subsequent work.

The result of the integration is illustrated in figure 2.11. Parameters are chosen such that $\Gamma = 2.0$, $T_e = 20\,\mathrm{keV}$, $M = 10^6\,M_\odot$, $a = 0.98$ and the disk accretes at Eddington luminosity. We assume the corona start at the inner edge of the disk and goes as far as the disk is able to keep it energetically. The figure 2.13 shows spectra for two values of the parameter α, which scales the amount of accretion energy that is transferred from the disk into corona, $\alpha = 1\%$ and $\alpha = 50\%$ and for comparison also the spectrum of the disk thermal emission only as if there was no corona at all. The spectrum clearly recovers the thermal part and the comptonized high-energy tail with a cut-off starting at approximately 100 keV. For any α approximately larger than 50%, the coverage factor is very small, less than a thousandth and pushes the power-law component down. One can also recognize the difference in the thermal part between the reference black-body spectrum and the $\alpha = 1\%$ spectrum with corona, where a noticable fraction of the thermal photons have been removed from this component and comptonized to form the power-law part of the corona.

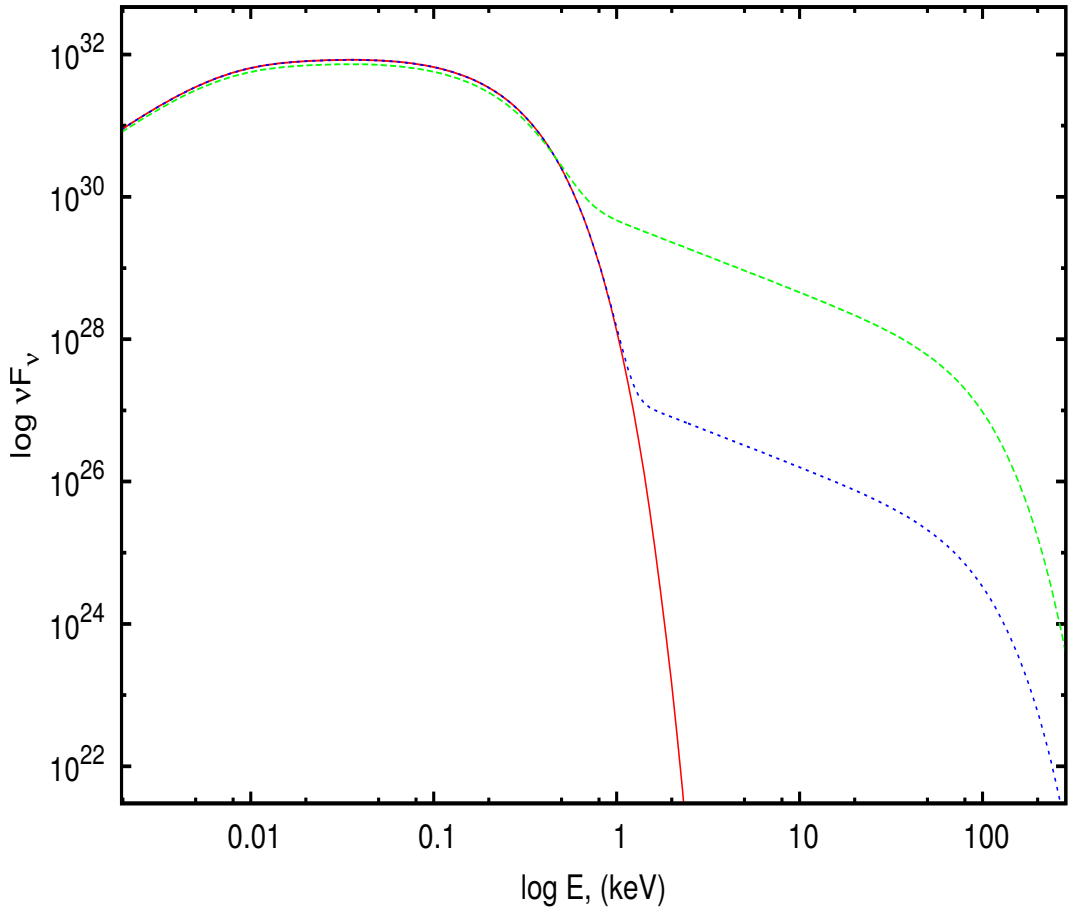

Figure 2.11: The global spectrum of the accretion disk of the black hole with the mass $M = 10^6 M_\odot$, black-hole spin $a = 0,98$, temperature of electrons in the corona $T_e = 20$keV and photon index $\Gamma = 2$. Spectrum is drawn for two values of parameter $\alpha = 0,5\%$ (blue dotted line), $\alpha = 0,01\%$ (green dotted line), also the black body spectrum with no corona attended is shown with red solid line.

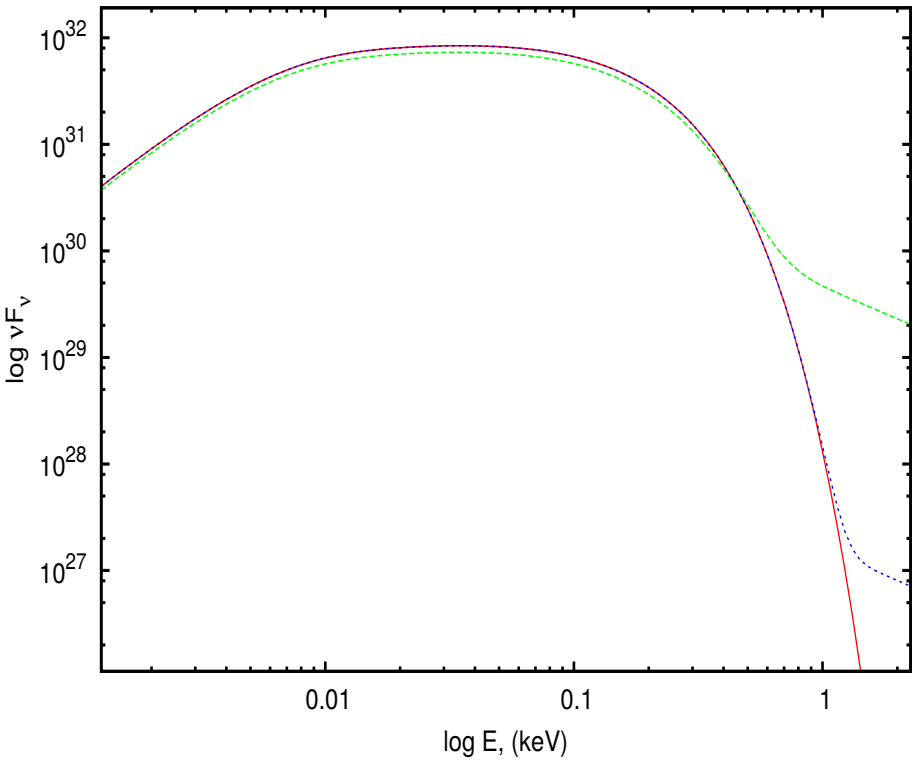

Figure 2.12: Black body part of the global spectrum of the accretion disk of the black hole with the mass $M = 10^6 M_\odot$, black-hole spin $a = 0,98$, temperature of electrons in the corona $T_e = 20$keV and photon index $\Gamma = 2$.

Conclusion

According to the widely accepted hypothesis a supermassive black hole is believed to be in the center of an active galaxy. Presence of a supermassive black hole in the center of AGN is responsible for its activity in X-ray range through an accretion process. There is a number of hypotheses on the origin of X-ray emission from AGN. In this thesis we supported one that assumes it to be originated in the formation above the accretion disk named corona. As we presented in the first chapter, corona has a large influence on the observed spectra from AGN. Depending on the parameters of corona, such as its optical depth, temperature of the electrons in the corona or geometry of the corona, observed spectra have broad variations and can be very different.

We focused on 'sandwich' geometry of corona and elaborated an interaction between the accretion disk and the corona through the equations of energy balance. However, from our simulation it followed that such a configuration of corona can not be a succesful physical model and does not correlate with observations. In further we had to define covering factor of corona, where the covering factor can be either time-factor, or space-factor. We considered this covering factor to be a space-factor, thus, we assumed 'patchy' geometry of corona. For 'patchy' geometry of corona we also elaborated energy balance between the disk and corona. From our simulation 'patchy' corona appeared to be more reliable physical model than 'sandwich'-like corona.

Finally, we managed to obtain the global model spectrum that can be observed under assumptions of 'patchy'-like corona. We may conclude that 'patchy' model of corona is a truthworhty physical model, that can compete with other possible configurations of corona and potentially bring successful results.

Bibliography

C. Done. Observational characteristics of accretion onto black holes. IAC winter school lecture notes, 2010.

M. Dovciak and C. Done. Minimum X-ray source size for a lamp-post corona in light-bending models for AGN. In *The Extremes of Black Hole Accretion*, page 26, July 2015. URL `http://adsabs.harvard.edu/abs/2015ebha.confE..26D`.

M. Dovciak, V. Karas, and T. Yaqoob. An extended scheme for fitting X-ray data with accretion disk spectra in the strong gravity regime. *The Astrophysical Journal Supplement Series*, 153:205–221, 2004.

A. C. Fabian. Strong gravity effects: X-ray spectra, variability and polarimetry. In *Black holes from stars to galaxies - across the range of masses*, number 238. International Astronomical Union, 2006.

J. Frank, A. King, and D. Raine. *Accretion power in astrophysics*. Cambridge University Press, 2002. ISBN 0-511-07597-9.

F. Haardt and L. Maraschi. A two-phase model for the X-ray emission from Seyfert galaxies. *The Astrophysical Journal*, 380:L51–L54, 1991.

F. Haardt, L. Maraschi, and G. Ghisellini. A model for the X-ray and ultraviolet emission from Seyfert galaxies and galactic black-holes. *The Astrophysical Journal*, 432:L95–L99, 1994.

C. Hazard, B. Mackey, M., and J. Shimmins, A. Investigation of the radio source 3C 273 by the method of lunar occultations. *Nature*, 197:1037–1039, 1963.

S. Kato, J. Fukue, and S. Mineshige. *Black-hole accretion disks*. Kyoto University Press, 1998. ISBN 4-87698-053-5 C3044.

D. Lynden-Bell and F. E. Pringle. The evolution of viscous disks and the origin of the nebular variables. *Monthly Notices of the Royal Astronomical Society*, 168:603–637, 1974.

J. Malzac. X-ray corona of X-ray binaries (and AGN). In *International Journal of Modern Physics Conference Series*, volume 8 of *International Journal of Modern Physics Conference Series*, pages 73–83, Heraklion, Crete, Greece, 2018. The 9th Fero meeting. Finding Extreme Relativistic Objects. doi: 10.1111/jmi.12720. URL `http://fero9.physics.uoc.gr/JMalzac.pdf`.

K. Nandra and K. A. Pounds. Ginga observations of the X-ray spectra of Seyfert galaxies. *Monthly Notices of the Royal Astronomical Society*, 268:405–429, 1994.

J. Poutanen and R. Svensson. The two-phase corona model for AGN and X-ray binaries : how to obtain exact solutions. *The Astrophysical Journal*, 470: 249–268, 1996.

J. N. Reeves and M. J. L. Turner. X-ray spectra of a large sample of quasars with ASCA. *Monthly Notices of the Royal Astronomical Society*, 316:234–248, 2000.

M. Schmidt. 3C 273: a star-like object with large red-shift. *Nature*, 197:1040, 1963.

N. I. Shakura and R. A. Sunyaev. Black holes in binary systems. Observational appearance. *Astronomy & Astrophysics*, 24:337–355, 1973.

B. A. Stern, J. Poutanen, R. Svensson, M. Sikora, and M. C. Begelman. On the geometry of the X-ray - emitting region in Seyfert galaxies. *The Astrophysical Journal*, 449:L13, 1995.

A. A. Zdziarski, W. N. Johnson, and P. Magdziarz. Broad-band gamma-ray and X-ray spectra of NGC 4151 and their implications for physical processes and geometry. *Monthly Notices of the Royal Astronomical Society*, 283:193–206, 1996.

P. T. Zycki, C. Done, and D. A. Smith. The May 1989 outburst of the soft X-ray transient GS 2023+338 (V404 Cyg). *Monthly Notices of the Royal Astronomical Society*, 309:561–575, 1999.

List of Figures